(16) NUMERICAL MODEL OF TIDAL FLOW AND EUTROPHICATION IN A TWO-LAYERED DENSITY STRATIFIED WATERBODY

密度二成層場における潮流と富栄養化の数値モデル

Haisheng JIN[1], Shinji EGASHIRA[1] and K.W.CHAU[2]
金 海生[1], 江頭 進治[1], 周 国英[2]

ABSTRACT; The integration of hydrodynamic and water quality models is preferable in modeling eutrophication. A two-layered, 2-D finite difference model for tidal flow and eutrophication in a two-layered density stratified waterbody is presented. The model is based upon numerically-generated, boundary-fitted orthogonal curvilinear coordinates. Nine water quality constituents — Chl-a, DO, CBOD, organic nitrogen, NH_4, NO_2+NO_3, organic phosphorus, PO_4 and zooplankton are included. SOD and nutrient releases from sediment are incorporated as descriptive inputs. The computed results on both hydrodynamic and water quality parameters are compared with the measurements in Tolo Harbour, Hong Kong. The computation for neglecting the density stratification is also conducted. It shows that the effects of density stratification on the vertical transport of both momentum and water quality parameters are evaluated reasonably. The computed results reproduce correctly the algae dynamics, nutrient kinetics, the bottom waters' extreme oxygen depletion and anoxic conditions.
KEYWORDS; Eutrophication, Tidal flow, Density stratification, Algae dynamics, Nutrient kinetics, CCHL

1. INTRODUCTION

Nutrients in kraft pulp mill effluent have resulted in major changes in the level of algal productivity in some rivers in western North America[1]. Since 1977, algal bloom in Biwa lake of Japan has usually occurred in early summer[2]. In Hong Kong, most of the coastal waters have excessive nutrient contents with high eutrophic potential and the development of algal blooms including red tides[3]. Many of these problems, including bottom-water anoxia, decline in fisheries, loss of aquatic vegetation, etc., are associated with eutrophication. It is now one of the most important water quality problems all over the world and has been attended seriously. In the past decades, much effort and money have been spent on combating it. Much research on eutrophication control and modeling has been conducted in recovering the equilibrium of ecosystem[4-6].

An eutrophication model describes the balance of mass and energy in an ecosystem. The mass and energy transformations are regulated by processes such as growth, respiration, mortality, and decomposition. These in turn are governed by environmental quality parameters such as flow, temperature, solar radiation, toxicity, nutrients, etc. The system is highly coupled, as the energy and mass balance for individual constituents is invariably linked to several others. Nowadays the forefronts of the modeling are the integration of hydrodynamic and water quality models. Moreover, the incorporation of sediment layers is indispensable for investigating the long-term recovery of an ecosystem.

Density stratification obstructs the connection between benthic grazers and near-surface biomass by inhibiting vertical mixing[7]. A three-dimensional model represents actually water flow and pollutant transport in a density stratified natural waterbody but it is resource demanding and computationally intensive. In many cases, density stratification can be evaluated as a two-layered system with a definite mesolimnion. Flow and transport in both layers may be in itself considered vertical homogeneously. It is then appropriate to describe the phenomenon in layer-averaged 2-D as depth-averaged model, except on the interaction between two layers. In

[1] Dept. of Civil & Environ. Engrg., Faculty of Science and Engrg., Ritsumeikan Univ., 1-1-1 Noji-higashi, Kusatsu, Shiga 525
[2] Dept. of Civil & Structrual Engineering, Hong Kong Polytechnic University, Hung Hom, Kowloon, HONG KONG

this study, a two-layered, 2-D numerical tidal flow and eutrophication model is proposed. Referring to the *in situ* sampling analysis, the sediment oxygen demand and nutrient release from sediment are incorporated. Some kinetic parameters are discussed and are calibrated by the scenario in Tolo Harbour of Hong Kong. Long term time-series results of the simulation and measurement are reported.

2. FRAMEWORK OF THE MODEL

The governing equations solved in the model, apart from the interaction on mass and momentum between the layers, are similar to, and are derived in a similar way to, the depth-averaged method[8]. In shallow areas in which position of the layer interface (Z_0) is equal to or lower than the bed level (Z_b), the bottom layer vanishes and the surface layer is only employed. An unified numerically-generated boundary-fitted orthogonal curvilinear coordinates is used for both the surface and the bottom layer. A "staggered" grid system is adopted, in which the water surface level (ζ) and scalar variables are calculated at the same node, and the components of vectors are "staggered" each other[9].

For all variables in this paper, subscript "u" and "l" designate the quantity in the upper and the lower layer respectively; subscript "0", "s" and "b" denote the value at the layer interface, at free surface and at bed respectively. k=index of layer: k='u' or 'l'. Notation $X_{y,20}$ means value of X_y at temperature 20°C and the notation θ is the relevant temperature correction coefficient. The definition of layer-averaged variables in detail can be found in ref.(9).

2.1 Governing equations for hydrodynamics

The differential equations in orthogonal curvilinear coordinates are expressed as:

$$Ct_k + \frac{1}{g_{11}g_{22}}\left[\frac{\partial(g_{22}h_k u_k^*)}{\partial\xi} + \frac{\partial(g_{11}h_k v_k^*)}{\partial\eta}\right] = 0, \quad Ct_u = \partial\zeta/\partial t - w_0 \quad \text{and} \quad Ct_l = -\partial Z_b/\partial t + w_0 \tag{1}$$

$$\frac{\partial(h_k u_k^*)}{\partial t} + \frac{1}{g_{11}g_{22}}\left\{\frac{\partial[g_{22}h_k(u_k^{*2} - \sigma_{1k})]}{\partial\xi} + \frac{\partial[g_{11}h_k(u_k^* v_k^* - \tau_{21k})]}{\partial\eta} + h_k\left[(v_k^* u_k^* - \tau_{12k})\frac{\partial g_{11}}{\partial\eta} - (v_k^{*2} - \sigma_{2k})\frac{\partial g_{22}}{\partial\xi}\right]\right\} = -\frac{h_k g}{g_{11}}\frac{\partial\zeta}{\partial\xi} + M_{\xi k}, \quad M_{\xi u} = w_0 u_0^* + (\tau_{s\xi} - \tau_{0\xi})/\rho - (h_u^2 g/2\rho_u g_{11})\partial\rho_u/\partial\xi \tag{2}$$

$$\text{and} \quad M_{\xi l} = -w_0 u_0^* + (\tau_{0\xi} - \tau_{b\xi})/\rho - (h_l g/\rho_l g_{11})(h_u \partial\rho_u/\partial\xi + 0.5 h_l \partial\rho_l/\partial\xi)$$

and a corresponding equation for η-component of the momentum, where u_k^* and v_k^* are the ξ and η components of averaged velocity in k-th layer; h_u (=ζ-Z_0) and h_l (=Z_0-Z_b) are the water depth in the surface and the bottom layer; u_0^*, v_0^* and w_0 are the ξ, η and z (positive vertically upward) components of velocity at the layer interface, respectively; ρ, ρ_u and ρ_l are the average density of water column, the density of water in the surface and the bottom layer; ρ=(ρ_u+ρ_l)/2; g is the acceleration due to gravity. σ_{1k}, σ_{2k}, τ_{12k} and τ_{21k} are the kth-layer-averaged effective stresses describing diffusion and dispersion. g_{11} and g_{22} are the orthogonal coordinate transformation relationships[9].

$\tau_{s\xi}$, $\tau_{0\xi}$ and $\tau_{b\xi}$ are the ξ–components of shear stress on the water surface, on the layer interface and on the bed, respectively. τ_s is ignored here. τ_b is expressed empirically as depth-averaged method except its direction according to velocity components in the bottom layer[9]. Referring to the Prandtl's mixing length theory and the empirical logarithmic velocity profile, τ_0 is calculated by

$$\frac{\tau_{0\xi}}{\rho} = \left(\varepsilon_m \frac{\partial u^*}{\partial z}\right)_{z=Z_0} \approx \varepsilon_m \frac{u_u^* - u_l^*}{\delta}, \quad \varepsilon_m = \varepsilon_{m0}(1+10\mathrm{Ri})^{0.5} \text{ and } \varepsilon_{m0} = \kappa h_l\left(1 - \frac{h_l}{h}\right)u_* \tag{3}$$

where ε_m is the vertical turbulent viscosity coefficient; ε_{m0} is the ε_m at the interface for the case without density stratification; κ (≈0.4) is the von Karman constant; h (=h_u+h_l) is the total water depth; u_* is the friction velocity; δ is the mixing layer thickness at the interface and is approximated by $\delta \approx \kappa h_l(1 - h_l/h)^{1/2}$. Ri is the gradient Richardson number at the interface:

$$Ri = -\frac{g}{\rho}\frac{\partial\rho/\partial z}{(\partial u/\partial z)^2} \approx \frac{\rho_l - \rho_u}{\rho}\frac{g\delta}{(u_u^* - u_l^*)^2 + (v_u^* - v_l^*)^2} \tag{4}$$

In the following simulations, ρ is estimated to be a function of local water temperature (T) and salinity (S). Field data instead of predictions are employed for T and S. For future research, it is much better to predict T and S simultaneously for capturing the density stratification precisely.

2.2 Transport equations of water quality variables

Organic carbon, organic nitrogen, NH_4-N, NO_2+NO_3-N, organic phosphorus, PO_4-P, DO, phytoplankton and zooplankton are simulated. Organic carbon is represented by its equivalent CBOD. Phytoplankton is characterized by its gross level — Chlorophyll-a. Zooplankton is represented by its organic carbon equivalence. Organic nitrogen is divided into particulate and dissolved phases by a dissolved fraction — f_{DON}, so is organic phosphorus by f_{DOP}. f_{DON} and f_{DOP} are calibrated on the basis of the field measurements[3]. NH_4, NO_2+NO_3 and PO_4 are considered as the available nutrients by phytoplankton uptake. The field data show that silicate is plentiful[3] and is excluded as a limiting nutrient. PO_4 is also divided into particulate and dissolved phases by a fraction —f_{DPO_4} and its dissolved phase is available for phytoplankton uptake. $(1-f_{DPO_4})$ is the fraction sorbed by suspended solid. f_{DPO_4} is calibrated with reference to Ambrose *et al.*'s analysis[5].

A general transport equation for layer-averaged concentration of each water quality variable reads:

$$\frac{\partial(h_k\varphi_k)}{\partial t} + \frac{1}{g_{11}g_{22}}\{\frac{\partial}{\partial\xi}[g_{22}h_k(u_k^*\varphi_k - \frac{\Gamma_{\xi,k}}{g_{11}}\frac{\partial\varphi_k}{\partial\xi})] + \frac{\partial}{\partial\eta}[g_{11}h_k(v_k^*\varphi_k - \frac{\Gamma_{\eta,k}}{g_{22}}\frac{\partial\varphi_k}{\partial\eta})]\} = \Phi_{\varphi,k}\,,$$
$$\Phi_{\varphi,u} = w_0\varphi_0 + Flux_{s,\varphi} - Flux_{0,\varphi} + S_{\varphi,u} \quad \text{and} \quad \Phi_{\varphi,l} = -w_0\varphi_0 + Flux_{0,\varphi} - Flux_{b,\varphi} + S_{\varphi,l} \tag{5}$$

where φ_k is the kth-layer-averaged concentration of a water quality variable and it may represent phytoplankton, organic nitrogen, DO, etc.; φ_0 is the concentration of φ at the layer interface, $\varphi_0 = \varphi_l$ if $w_0 \geq 0$ otherwise $\varphi_0 = \varphi_u$; w_0 is calculated from layer-averaged continuity equation[9]; $\Gamma_{\xi,k}$ and $\Gamma_{\eta,k}$ are the longitudinal and transverse dispersive (including diffusion) coefficients in the kth-layer. $Flux_{s,\varphi}$, $Flux_{b,\varphi}$ and $Flux_{0,\varphi}$ are the vertical diffusive fluxes of φ across the water surface, the bed and the interface respectively. $Flux_{s,\varphi}$ is assumed to be zero. It is difficult to calculate $Flux_{b,\varphi}$ directly because sediment-overlying water interactions are not predicted in the model. $Flux_{b,\varphi}$ is approximately considered in SOD, nutrient release from sediments, etc., as a descriptive input. $Flux_{0,\varphi}$ is calculated by

$$Flux_{0,\varphi} = \left(\Gamma_m\frac{\partial\varphi}{\partial z}\right)_{z=Z_0} \approx \Gamma_m\frac{\varphi_u - \varphi_l}{\delta}\,, \quad \Gamma_m = \Gamma_{m0}(1+\frac{10}{3}Ri)^{-1.5}\,, \quad \Gamma_{m0} = \frac{\varepsilon_{m0}}{\sigma_t} \tag{6}$$

in which Γ_m is the flux diffusive coefficient, Γ_{m0} is the Γ_m for the case without density stratification, and σ_t ($\approx$0.9) is the turbulent Schmidt number[10].

$S_{\varphi,k}$ may represent the reaction kinetics, settling, sediment release, and external sources and/or sinks in the kth-layer. $S_{\varphi,k}$ for each water quality variable is listed in table 1[4,5]. The notation and its unit used in the model for each water quality variable are defined in the table. The definitions of relevant kinetic parameters and saturation constants are described in table 2. Their values used in the following simulation are also listed.

The quantities of water quality variables decrease due to the corresponding settling — w_{SA}, w_{SZ}, w_{SN}, w_{SP}, w_{SPO_4} and w_{SBOD} (m/day). The algal growth relates to multiple factors, including available nutrients, water temperature, solar radiation, zooplankton grazing, tidal flushing and so on. Organic nitrogen undergoes a bacterial decomposition whose end-product is ammonia (NH_4-N). Organic phosphorus converts to inorganic phosphorus (mainly orthophosphate phosphorus — PO_4-P) by mineralization. Saturating recycle expressions[5] for the hydrolysis and bacterial decomposition of organic nitrogen (k_{34}) and the mineralization of organic phosphorus (k_{67}) are chosen:

$$k_{34} = k_{34,20}\theta^{T_k-20}\frac{A_k}{K_{mpc}+A_k}\,, \qquad k_{67} = k_{67,20}\theta^{T_k-20}\frac{A_k}{K_{mpc}+A_k} \tag{7}$$

Table 1. Definition of water quality variables and their source terms in the 2-layered, 2-D eutrophication model

Description	Notation	$S_{\varphi,k}$ (k='u' for the surface layer and k='l' for the bottom layer)	
Phyplankton	A_k (μgChl-a/l)	$h_u(\mu_{A,u} - r_A - M_A - C_g Z_u)A_u - w_{SA}A_u + s_{A,u}$	$h_l(\mu_{A,l} - r_A - M_A - C_g Z_l)A_l - w_{SA}(A_l - A_u) + s_{A,l}$
Zooplankton	Z_k (mgZooplC/l)	$h_u(\alpha_2 \frac{K_Z}{K_Z + A_u} C_g \alpha_{12} A_u - r_Z - M_Z)Z_u - w_{SZ}Z_u + s_{Z,u}$	$h_l(\alpha_2 \frac{K_Z}{K_Z + A_l} C_g \alpha_{12} A_l - r_Z - M_Z)Z_l - w_{SZ}(Z_l - Z_u) + s_{Z,l}$
Organic Nitrogen	N_k (μgN/l)	$h_u[f_{ON}\alpha_{13}(r_A + M_A)A_u + f_{ON}\alpha_{23}(r_Z + M_Z)Z_u - k_{34}N_u] - w_{SN}(1 - f_{DON})N_u + s_{N,u}$	$h_l[f_{ON}\alpha_{13}(r_A + M_A)A_l + f_{ON}\alpha_{23}(r_Z + M_Z)Z_l - k_{34}N_l] - w_{SN}(1 - f_{DON})(N_l - N_u) + SR_N + s_{N,l}$
NH_4-N	$NH_{4,k}$ (μgN/l)	$h_u\{(1 - f_{ON})[\alpha_{13}(r_A + M_A)A_u + \alpha_{23}(r_Z + M_Z)Z_u] + k_{34}N_u - f_{pref,u}\alpha_{13}\mu_{A,u}A_u - k_N NH_{4,u}\} + s_{NH_4,u}$	$h_l\{(1 - f_{ON})[\alpha_{13}(r_A + M_A)A_l + \alpha_{23}(r_Z + M_Z)Z_l] + k_{34}N_l - f_{pref,l}\alpha_{13}\mu_{A,l}A_l - k_N NH_{4,l}\} + SR_{NH_4} + s_{NH_4,l}$
NO_2+NO_3-N	$NO_{23,k}$ (μgN/l)	$h_u[k_N NH_{4,u} - (1 - f_{pref,u})\alpha_{13}\mu_{A,u}A_u - k_{55}NO_{23,u}] + s_{NO_{23},u}$	$h_l[k_N NH_{4,l} - (1 - f_{pref,l})\alpha_{13}\mu_{A,l}A_l - k_{55}NO_{23,l}] + SR_{NO_{23}} + s_{NO_{23},l}$
Organic Phosphorus	P_k (μgP/l)	$h_u\{f_{OP}[\alpha_{16}(r_A + M_A)A_u + \alpha_{26}(r_Z + M_Z)Z_u] - k_{67}P_u\} - w_{SP}(1 - f_{DOP})P_u + s_{P,u}$	$h_l\{f_{OP}[\alpha_{16}(r_A + M_A)A_l + \alpha_{26}(r_Z + M_Z)Z_l] - k_{67}P_l\} - w_{SP}(1 - f_{DOP})(P_l - P_u) + SR_P + s_{P,l}$
PO_4-P	$PO_{4,k}$ (μgP/l)	$h_u\{(1 - f_{OP})[\alpha_{16}(r_A + M_A)A_u + \alpha_{26}(r_Z + M_Z)Z_u] - \alpha_{16}\mu_{A,u}A_u + k_{67}P_u\} - w_{SPO_4}(1 - f_{DPO_4})PO_{4,u} + s_{PO_4,u}$	$h_l\{(1 - f_{OP})[\alpha_{16}(r_A + M_A)A_l + \alpha_{26}(r_Z + M_Z)Z_l] - \alpha_{16}\mu_{A,l}A_l + k_{67}P_l\} - w_{SPO_4}(1 - f_{DPO_4})(PO_{4,l} - PO_{4,u}) + SR_{PO_4} + s_{PO_4,l}$
CBOD	BOD_k (mgO_2/l)	$h_u[\frac{32}{12}(\alpha_{18}M_A A_u + M_Z Z_u) - (\frac{5}{4}\frac{32}{14}k_{55}NO_{23,u} + k_C BOD_u)] - w_{SBOD}BOD_u + s_{BOD,u}$	$h_l[\frac{32}{12}(\alpha_{18}M_A A_l + M_Z Z_l) - (k_C BOD_l + \frac{5}{4}\frac{32}{14}k_{55}NO_{23,l})] - w_{SBOD}(BOD_l - BOD_u) + s_{BOD,l}$
Dissolved Oxygen	DO_k (mgO_2/l)	$h_u\{k_a(DO^s - DO_u) + \frac{32}{12}[\alpha_{18}(\mu_{A,u} - r_A)A_u - r_Z Z_u] + \frac{48}{14}\alpha_{13}(1 - f_{pref,u})A_u - (k_C BOD_u + \frac{64}{14}k_N NH_{4,u})\} + s_{DO,u}$	$h_l\{\frac{32}{12}[\alpha_{18}(\mu_{A,l} - r_A)A_l - r_Z Z_l] + \frac{48}{14}\alpha_{13}(1 - f_{pref,l})A_l - (k_C BOD_l + \frac{64}{14}k_N NH_{4,l})\} - SOD + s_{DO,l}$

Note: SOD = Sediment Oxygen Demand (gO_2/m^2day). SR_N, SR_{NH_4}, $SR_{NO_{23}}$ (mgN/m^2day), SR_P and SR_{PO_4} (mgP/m^2day) are the organic nitrogen, NH_4-N, NO_2+NO_3-N, organic phosphorus and PO_4-P released from sediment, respectively. $s_{A,k}$ ($mgChl\text{-}a/m^2day$), $s_{Z,k}$ ($gZooplC/m^2day$), $s_{N,k}$, $s_{NH_4,k}$, $s_{NO_{23},k}$ (mgN/m^2day), $s_{P,k}$, $s_{PO_4,k}$ (mgP/m^2day), $s_{BOD,k}$ and $s_{DO,k}$ (mgO_2/m^2day) are the corresponding direct sources and are determined according to the pollutant loadings. DO^s =DO saturation concentration (mgO_2/l).

Table 2. Kinetic and stoichiometric parameters used in the 2-layered, 2-D eutrophication model

Parameter	Description (its unit)	Value (and θ)
$\mu_{A,k}^{max}$	Maximum phytoplankton growth rate (day^{-1})	2.10 (1.066)[b]
K_{mNN}	Half-saturation const. for nitrogen uptake (μgN/l)	15.0[b]
K_{mNP}	Half-saturation const. for phosphorus uptake (μgP/l)	1.50
K_{mpc}	Half saturation const. for algae effect on mineralization (μgChl-a/l)	10.0
K_{NIT}	Half saturation DO const. for oxygen limitation of nitrification (mgO_2/l)	2.0[a]
K_{NO}	Half-max. DO const. for oxygen limitation of denitrification (mgO_2/l)	0.1[a]
K_{BOD}	Half saturation DO const. for CBOD deoxygenation (mgO_2/l)	0.5[a]
r_A	Endogenous respiration rate of algae (day^{-1})	0.05 (1.08)[b]
M_A	Mortality rate of algae (day^{-1})	0.1
C_g	Grazing (filtering) rate of zooplankton (liters/mgZooplC/day)	0.30 (1.066)
r_Z	Endogenous respiration rate of zooplankton (day^{-1})	0.02 (1.045)[c]
M_Z	Mortality rate of zooplankton (day^{-1})	0.1[b]
K_Z	Half-max.-efficiency food level for zoopl. filtering (μg Chl-a/l)	12.0
k_{34}	Conversion efficiency of organic nitrogen to NH_4-N (day^{-1})	0.05 (1.08)[b]
k_N	Nitrification rate of NH_4 to NO_3 via NO_2-N (day^{-1})	0.05 (1.08)
k_{55}	Denitrification rate (day^{-1})	0.09 (1.045)[a]
k_{67}	Conversion efficiency of organic-P to PO_4-P (day^{-1})	0.03 (1.08)
k_C	Decay rate of carbonaceous BOD (day^{-1})	0.23 (1.047)[b]
$BOD_{u\text{-}5}$	Ratio of the ultimate to 5-day carbonaceous BOD	1.54
α_{12}	Assimilated carbon per unit algae mass ingested (mean CCHL)	112.5
α_2	Zoopl. assim. efficiency (mgZooplC assimilated/mgZooplC ingested)	0.6[b]
α_{13}	Stoich. ratio of cell nitrogen to algae Chl-a (μgN/μgChl-a)	10.0[b]
α_{23}	Stoich. ratio of cell nitrogen to zoopl. carbon (μgN/μgZooplC)	α_{13}/CCHL
α_{16}	Stoich. ratio of phosphorus to algae Chl-a (μgP/μgChl-a)	1.0
α_{26}	Stoich. ratio of phosphorus to zoopl. carbon (μgP/μgZooplC)	α_{16}/CCHL
α_{18}	Stoich. ratio of algae to organic carbon (mgC/mgChl-a)	CCHL
f_{ON}	Fraction of dead algae and zoopl. recycled to organic-N	0.5[b]
f_{OP}	Fraction of dead algae and zoopl. recycled to organic-P	0.5[a]
f_{DON}	Fraction of dissolved organic-N in the totals	0.55
f_{DOP}	Fraction of dissolved organic-P in the totals	0.55
f_{DPO_4}	Fraction of dissolved PO_4-P in the totals	0.75
Reference: [a] Ambrose et al. (1988), [b] Lee et al. (1991), [c] Thomann and Mueller (1987)		

Ammonia nitrogen, in the presence of nitrifying bacteria and oxygen, is converted to NO_3-N (k_N): $NH_3^+ + 2O_2 \rightarrow NO_3 + H_2O + H^+$. Denitrification ($k_{55}$) occurs under anaerobic condition: $5CH_2O + 5H_2O + 4NO_3 + 4H^+ \rightarrow 5CO_2 + 2N_2 + 12H_2O$. CBOD decreases due to stabilization (k_C).

$$k_N = k_{N,20}\theta^{T_k-20}\frac{DO_k}{K_{NIT}+DO_k}, \quad k_{55} = k_{55,20}\theta^{T_k-20}\frac{K_{NO}}{K_{NO}+DO_k}, \quad k_C = k_{C,20}\theta^{T_k-20}\frac{DO_k}{K_{BOD}+DO_k} \tag{8}$$

Both NH_4 and NO_2+NO_3 are available for algae uptake, however, the preferred form is NH_4-N for physiological reasons. The ammonia preference is described by a factor — $f_{pref,k}$[5]:

$$f_{pref,k} = \frac{NH_{4,k}}{K_{mNN}+NO_{23,k}}\left(\frac{NO_{23,k}}{K_{mNN}+NH_{4,k}} + \frac{K_{mNN}}{NH_{4,k}+NO_{23,k}}\right) \tag{9}$$

A byproduct of photosynthetic carbon fixation is the production of DO. An additional source of oxygen from algal growth occurs when the available ammonia nutrient source is exhausted and the phytoplankton begins to

utilize the available nitrate. For nitrate uptake, the initial step is a reduction to ammonia which produces oxygen as: $2NO_3 \rightarrow 2NH_3 + 3O_2$. DO increases by atmospheric reaeration (k_a, day^{-1}) because of the deviation from the saturation concentration — DO^s (mgO_2/l)[4]:

$$k_a = k_{a,20}(1.024)^{T_k-20}, \quad k_{a,20} = \begin{cases} \dfrac{3.9V^{0.5}}{h^{1.5}}, & W < 6.0m/s; \\ \dfrac{3.9V^{0.5}}{h^{1.5}} + \dfrac{0.728W^{0.5} - 0.317W + 0.0372W^2}{h}, & W \geq 6.0m/s \end{cases} \tag{10}$$

$$\ln DO^s = -139.3441 + \frac{1.5757\times10^5}{T_u+273.15} - \frac{6.6423\times10^7}{(T_u+273.15)^2} + \frac{1.2438\times10^{10}}{(T_u+273.15)^3} - \frac{8.6219\times10^{11}}{(T_u+273.15)^4} - S_u\left[1.7674\times10^{-2} - \frac{1.0754\times10}{T_u+273.15} + \frac{2.1407\times10^3}{(T_u+273.15)^2}\right] \tag{11}$$

where V is the depth-averaged velocity of flow in m/s; W is the wind speed in m/s at 10m above water surface; T_k (°C) and S_k (ppt) are the relevant water temperature and salinity.

(1) Algae dynamics and CCHL — the carbon to chlorophyll-a ratio

The growth and proliferation of algae is a result of the utilization and conversion of inorganic nutrients into organic plant material through the photosynthesis mechanism. A multiplicative expression[4] is assumed for the algae growth rate — μ_A:

$$\mu_{A,k} = \mu_{A,k}^{max} g(I)_k \min\left\{\frac{NH_{4,k}+NO_{23,k}}{K_{mNN}+NH_{4,k}+NO_{23,k}}, \frac{PO_{4,k}*f_{DPO_4}}{K_{mNP}+PO_{4,k}*f_{DPO_4}}\right\}, \quad \mu_{A,k}^{max} = \mu_{A,20}^{max}\theta^{T_k-20},$$
$$g(I)_u = \frac{2.718}{\gamma_u h_u}[e^{-\alpha_1} - e^{-\alpha_0}], \quad g(I)_l = \frac{2.718}{\gamma_l h_l}[e^{-\alpha_2} - e^{-\alpha_1}], \quad \alpha_0 = \frac{I_0}{I_s}, \quad \alpha_1 = \alpha_0 e^{-\gamma_u h_u}, \quad \alpha_2 = \alpha_1 e^{-\gamma_l h_l} \tag{12}$$

where I_0 and I_s are the incoming solar radiation intensity just below the surface and saturating light intensity, respectively; $\mu_{A,k}^{max}$ is the maximum growth rate of phytoplankton under optimal light and nutrient conditions; γ_k (m^{-1}) is the overall extinction coefficient in relevant layer and Lee *et al.*'s expression[6] is employed: $\gamma_k = 0.24 - 0.0057A_k + 0.145A_k^{1/2}$.

Phytoplankton may adjust its chlorophyll composition to adapt to the changes in solar radiation. Hence, I_s is determined to be the weighted average of the light intensity for previous three days: $I_s = 0.7I_1 + 0.2I_2 + 0.1I_3$, where I_i=0.5×(daily average visible light intensity beneath the surface) 'i' days earlier[6]. Moreover, a variable carbon to chlorophyll-a ratio — CCHL, based on the assumption that adaptive changes in carbon to chlorophyll occur so as to maximize the specific growth rate for ambient conditions of light and temperature[5], is determined: $CCHL = \alpha I_s / 2.718\mu_{A,k}^{max}$. $\alpha \cong 6.0$mgC/mgChl-a·ly according to Lee *et al.*'s experiment[6].

(2) Sediment oxygen demand (SOD) and sediment release of nutrients

SOD comprises two components; one results from the oxidation of sediment algal carbon (SOD_C) and the another results from the other processes (SOD_0):

$$SOD = SOD_C + SOD_0, \quad SOD_C = 32k_{Csedi}C_{sedi}/12, \quad SOD_0 = SOD_{0,20}\theta^{T_l-20}, \quad \theta = 1.047 \tag{13}$$

where k_{Csedi} [$= 0.15(1.047)^{T_l-20}$ day^{-1}] is the oxidation rate of sediment algal carbon; C_{sedi} (gC/m^2) is the sediment algal carbon (SAC) and is computed with the following equation:

$$\frac{dC_{sedi}}{dt} = \alpha_{sediCA} w_{SA} A_l - \frac{v_{sedi}}{h_{sedi}} C_{sedi} - k_{Csedi} C_{sedi} \tag{14}$$

in which α_{sediCA} (gC/gChl-a) is the SAC per unit algal mass settled and is taken as an average CCHL; v_{sedi} (m/day) is the sediment accumulation rate (part of SAC may be buried with time history) and h_{sedi} (m) is the thickness of the sediment layer. Herein, v_{sedi}/h_{sedi} =0.001 day^{-1}.

A detailed description of nutrient release from sediments is often significant for prediction models[4, 5, 11]. Such release occurs as a result of a gradient in nutrient concentration between the overlying water and the nutrient in the interstitial water of the sediment. The releases are taken into account as descriptive inputs.

2.3 Boundary and initial conditions, and numerical method

The bank is assumed to be impenetrable. The normal velocity is equal to zero and the tangential component, conforming to resistance law, is not zero. The normal gradients for all water quality variables are specified as zero. The concentrations for all water quality variables at the open boundary are given when water flows into the waterbody of interest, otherwise the normal gradients of concentrations are simply specified as zero. Upstream velocities and downstream tidal elevation are given. At the confluence of stream and tributary, velocity and concentrations for all water quality variables may be exactly specified.

The initial conditions in all the two layers are specified by interpolating the corresponding boundary conditions at the starting time.

A time-splitting scheme, with two fractional steps: (1) advection and diffusion, and (2) propagation and source terms, is used to solve numerically the governing equations for tidal flow[9]. Control-volume formulation[12] is employed to discretize the differential equations governing water quality processes.

The procedure of the solution in a time step is: the hydrodynamic equations are solved first, and then the equations for phytoplankton, zooplankton, organic nitrogen, NH_4-N, NO_2+NO_3-N, organic phosphorus, PO_4-P, CBOD and DO in sequence.

3. SIMULATION OF EUTROPHICATION IN TOLO HARBOUR, HONG KONG

The tidal flow and eutrophication in Tolo Harbour, Hong Kong, is simulated by the present method. Tolo Harbour is a nearly land-locked sea inlet with an area of about 52km^2 (fig.1). The averaged diurnal tidal difference is about 0.97m. Mean high and low tide elevations are 1.75m and 0.78m, respectively (M.C.D.—Metre Chart Datum). For most of the year, little freshwater is discharged into the harbour. During summer, however, a two-layered density stratified system is formed due to the solar radiation and rainfall. The measured water temperature and salinity are shown in fig.2[3].

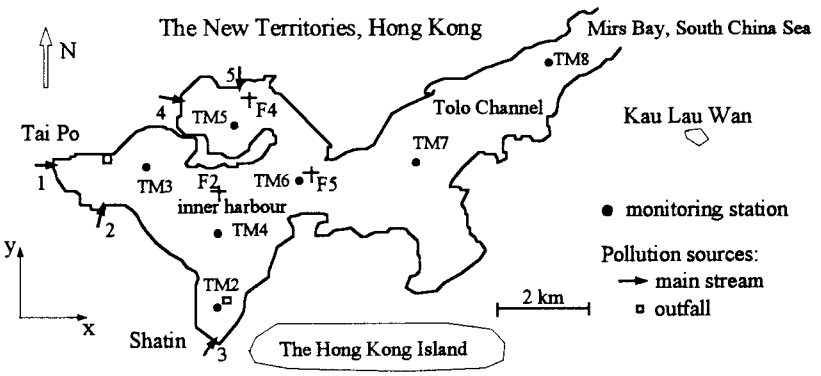

Fig.1 Schematic map of Tolo Harbour, Hong Kong

A boundary-fitted orthogonal curvilinear grid system with total of 580 grid cells is employed. The longitudinal grid size is about 110~710m and the transverse size about 60~530m. It was generated numerically by solving two elliptical equations. According to the measured data, the layer interface position is specified at Z_0=-6m (M.C.D.)[9].

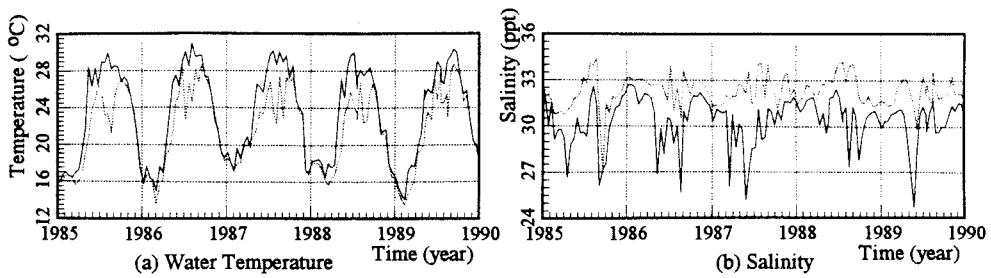

Fig.2 Water Temperature and Salinity in Tolo Harbour, Hong Kong (— surface, ··· bottom)

The solution of tidal flow has been verified previously. It has been shown that the effects of density stratification are represented fairly well in the solution[9]. The flow directions in the surface and the bottom layer are inconsistent, especially when the current is not too swift. Fig.3 displays the velocity hodographs at three locations for a typical semidiurnal tide. The Eulerian velocities in most of the harbour, especially in the outer area, i.e., in Tolo Channel, have a prevailing direction along the channel and its transverse component is very small relative to its longitudinal counterpart. In side coves, however, the directions in the surface layer are generally different from those in the bottom layer. The computed Lagrangian pathlines showed that the tidal excursion is dependent on the tidal type, especially in the inner harbour and side coves[9].

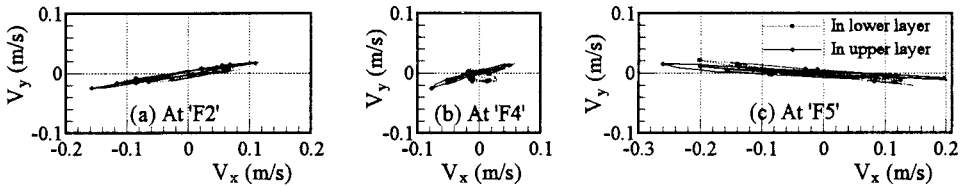

Fig.3 Computed velocity hodographs in Tolo Harbour, Hong Kong

In the following long term simulation, tidal level at the open boundary is predicted according to a harmonic analysis of a long series of observations at Kau Lau Wan using 42 tidal constituents.

The pollution sources comprise those from five main streams (fig.4) and those from outfalls of two sewage treatment plants at Shatin and Tai Po, which are taken as point-loadings. Non-point sources are scarce and they are not considered in the simulation[3, 13].

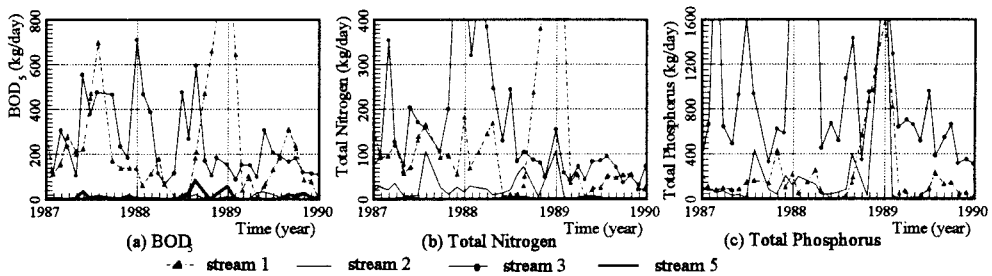

Fig.4 Pollutant loadings discharged into Tolo Harbour from streams

A relevant *in situ* study had been conducted simultaneously by Mr.F.L.Hua, *et al.* in Hong Kong Polytechnic University from June to October 1994 at five locations in Tolo Harbour. According to the analysis on 80 samples, the nutrient releases from sediment are: organic nitrogen ranging from 6 to 40 mgN/(m^2day) (about 16.8 on average); NH_4-N 18 to 205 mgN/(m^2day) (62.4); NO_2+NO_3-N -4.43 to 9.16 mgN/(m^2day) (0.212); organic phosphorus 0.17 to 1.61 mgP/(m^2day) (0.5); and PO_4-P 1.45 to 8.90 mgP/(m^2day) (2.65). $SOD_{0,20}$ is

between 0.47 and 1.24 $gO_2/(m^2day)$ and about 0.88 on average. As descriptive inputs, the mean quantities are used in the simulation.

The annual average of daily solar radiation intensity in Tolo Harbour is about 300 ly/day. Hourly I_o, issued by the Royal Observatory of Hong Kong, is imposed in the simulation.

The computed nutrient concentrations with the parameters listed in table 2 and measurements at TM8 in Tolo Harbour are shown in fig.5. The Chl-a and DO concentrations at three locations are displayed in fig.6. The results computed by the present model mimic the measured data in Tolo Harbour. In long-term simulations, it is difficult that the predictions by an ecosystem model always agree perfectly with the measurements. A reasonable examination of the numerical model is that its predictions should agree closely with the central trend of the observations. From this point of view, the above results demonstrate that the present model could reproduce reasonably the algal growth dynamics and nutrient kinetics in both the surface and the bottom layer. The peak concentrations of the nutrients (fig.5) which are related to higher pollutant loadings in early 1988 (fig.4) are predicted by the model.

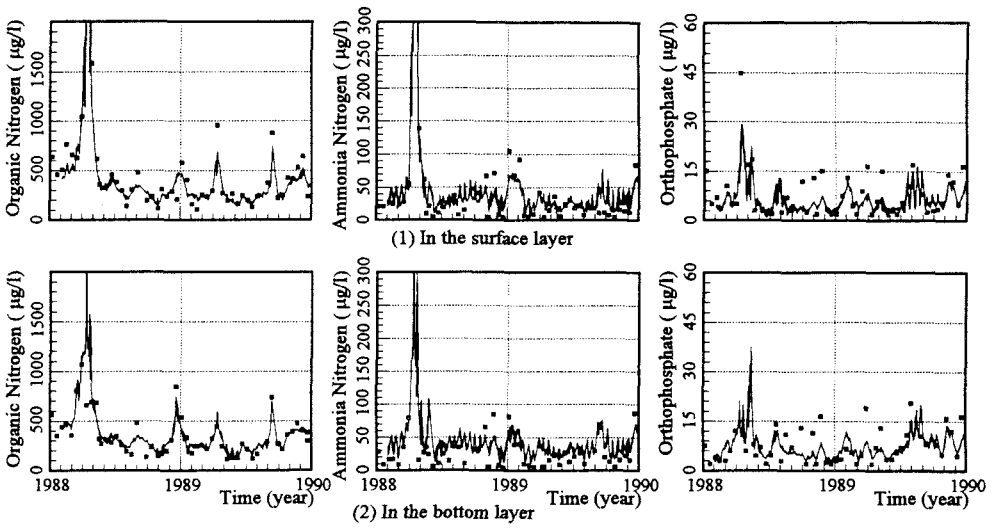

Fig.5 Nutrients at TM8 in Tolo Harbour, Hong Kong (— computed, ▪ measured)

The water quality processes in both the surface and the bottom layer in Tolo waters are almost similar except for their differences in magnitude. During January and February, the temperature is low and the solar radiation is weak, low Chl-a concentration and nearly saturated DO are the features of the waterbody. During Spring and early Summer, starting from March, the temperature rises and the solar radiation intensifies. The Chl-a can attain its annual maximum and the nutrients are rapidly depleted by the algal bloom. Meanwhile, the DO can maintain a super-saturated period due to photosynthesis and then rapidly decreases because of the activity of settled algal carbon as SOD. The bottom water anoxia may occur, even in the Tolo channel, and the anoxic condition may retain a prolonged period, especially in the inner harbour. From later summer to December, the lower Chl-a is maintained and the DO is restored gradually.

The stratification tendency of water quality parameters has been evaluated well by the present model. The surface water in the harbour is generally well oxygenated. However, extreme oxygen depletion and anoxic conditions, below 5% saturation, may appear throughout the whole bottom waters during summer (fig.6). These are caused by the high oxygen demand due to the decay of organic matter in the sediment at higher summer temperatures. The respiration of benthos further uses up the oxygen in the bottom water. Moreover, the weak turbulent mixing, due to the density stratification in the water column, prevents vertical mixing and replenishment of oxygen from the well aerated surface water to the bottom. The stratification almost diminishes during winter, however. Thus, the vertically uniform distribution of water quality may be attained.

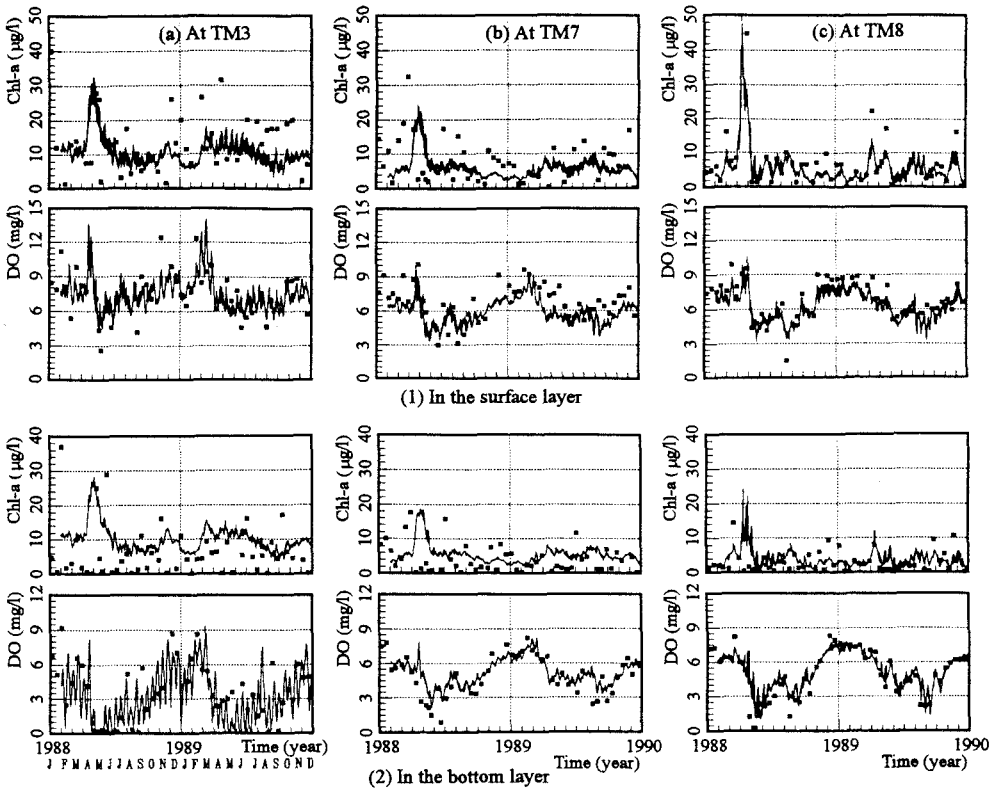

Fig.6 Chl-a and DO at different locations (— computed, ▪ measured)

Fig.7 shows the computed DO concentration at the three locations, in which the density stratification is ignored. The measured data in fig.7 are the same as those in fig.6. The stratification on the computed DO concentration in the water column tends to disappear in contrast with the measurements and the computed results in fig.6. It emphasizes that the density stratification plays an important role in the vertical mixing and the model is successful in handling its effects.

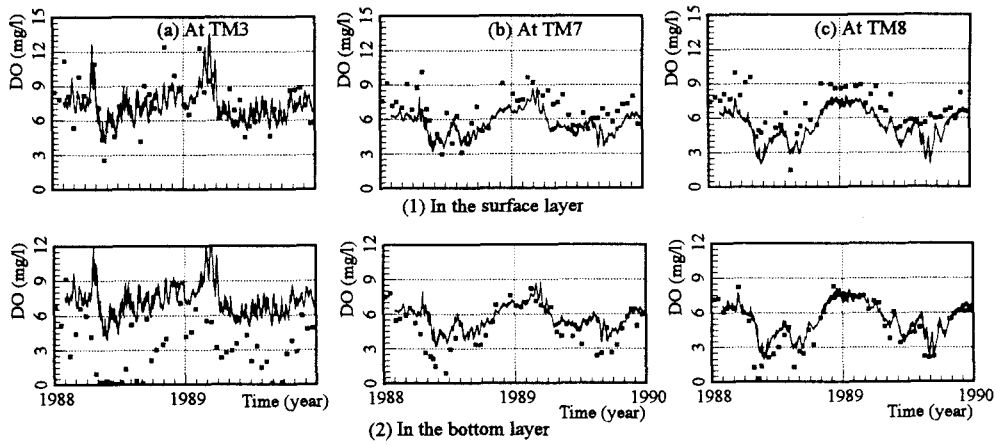

(— computed, ▪ measured)

Fig.7 The computed DO without consideration of the density stratification and the measurement

4. CONCLUSIONS

In modeling eutrophication, it is preferable to couple the hydrodynamic simulation with the water quality model and to take the effects of density stratification into account. A rigorous 2-D finite difference model, which describes two layer-averaged tidal flow and eutrophication in a two-layered density stratified waterbody, has been demonstrated. For adapting to the irregular boundaries of waterbody, the model is based upon the numerically-generated, boundary-fitted orthogonal curvilinear coordinates. The solution for the hydrodynamic parameters has been calibrated and verified by the previous study. Besides the hydrodynamic parameters, Chl-a, DO, CBOD, organic nitrogen, NH_4-N, NO_2+NO_3-N, organic phosphorus, PO_4-P and zooplankton, associated with eutrophication, are simulated. SOD and nutrient releases from sediment are incorporated in the model. The present method is applied to simulate the long term eutrophication process in Tolo Harbour, Hong Kong. The monitoring point-loadings and hourly solar radiation are employed in the simulation. The computational results represent correctly the algal dynamics, nutrient kinetics, the bottom waters' serious oxygen depletion and anoxic conditions. The model reproduces the unsteady layer-averaged 2-D eutrophication phenomena very well. The effects of density stratification on vertical transport of both momentum and water quality parameters are handled reasonably. The stratification on the computed DO concentration in the water column tends to disappear if the density stratification is ignored for the calculation.

ACKNOWLEDGEMENT

The EPD, the Royal Observatory and the Drainage Service Department of Hong Kong are gratefully acknowledged for providing the monitoring data in Tolo Harbour.

REFERENCES

1) Bothwell, M.L., "Eutrophication of rivers by nutrients in treated kraft pulp mill effluent", *Water Pollution Research Journal of Canada*, 27(3), 447-472, 1992.
2) SWEC (Secretariat of Water Environmental Conference of Biwa Lake and Yodo River), *To a favourable change of Biwa lake and Yodo river —A proposal*, Chap.2. 40-119, 1996.
3) EPDHK (Environmental Protection Dept., Hong Kong), *Marine water quality in Hong Kong: results from the EPD marine water quality monitoring programme for 1989*, EP/TR 3/90, 1990.
4) Thomann R.V. and Mueller J.A., *Principles of Surface Water Quality Modeling and Control*, Harper & Row, Publishers, New York, 1987.
5) Ambrose R.B., Wool T.A., Connolly J.P. and Schanz R.W., *WASP4*, EPA/600/3-87/039, U.S., 1988.
6) Lee J.H.W., Wu R.S.S., Cheung Y.K. and Wong P.P.S., "Forecasting of dissolved oxygen in marine fish culture zone", *J. of Envir. Engrg., ASCE*, 117(6), 816-833, 1991.
7) Yih Chia-Shun, *Stratified Flows*, Academic Press, 1980.
8) Abbott, M.B., *Computational Hydraulics*. Ashgate Publishing Limited, 1979.
9) Chau K.W. and Jin H.S., "Numerical solution of two-layered, 2-D tidal flow in boundary-fitted orthogonal curvilinear coordinate system", *Inter. J. for Num. Meth. in Fluids*, 21(11), 1087-1107, 1995.
10) Rodi W., *Turbulence Models and Their Application in Hydraulics, state-of-the-art*, IAHR Publication, DELFT, The Netherlands, 1980.
11) Di Toro Dominic M., Paquin P.R., Subburamu K., and Gruber D.A., "Sediment oxygen demand model: methane and ammonia oxidation", *J. of Envir. Engrg., ASCE*, 116(5), 945-986, 1990.
12) Patankar S.V., *Numerical Heat Transfer and Fluid Flow*, Hemisphere Publishing Corporation, 1980.
13) EPDHK (Environmental Protection Dept., Hong Kong), *River water quality in Hong Kong: results from the EPD river water quality monitoring programme for 1989 and 1990*, EP/TR 2/91, 1991.